Author Manuscript

Author Manuscript

Author Manuscript

Author Manuscript

HHS Public Access

Author manuscript

Mol Cancer Res. Author manuscript; available in PMC 2020 July 05.

Published in final edited form as:

Mol Cancer Res. 2020 July ; 18(7): 1004–1017. doi:10.1158/1541-7786.MCR-19-0669.

Targeting NAD+ biosynthesis overcomes panobinostat and bortezomib-induced malignant glioma resistance

Esther P. Jane[#1,2], **Daniel R. Premkumar**[#1,2,3], **Swetha Thambireddy**[1], **Brian Golbourn**[1], **Sameer Agnihotri**[1,2,3], **Kelsey C. Bertrand**[4], **Stephen C. Mack**[4], **Max I. Myers**[1], **Ansuman Chattopadhyay**[5], **D. Lansing Taylor**[6,7,8], **Mark E. Schurdak**[6,7,8], **Andrew M. Stern**[7,8], **Ian F. Pollack**[1,2,3]

[1]Department of Neurosurgery, Pittsburgh, Pennsylvania, U.S.A.

[2]University of Pittsburgh School of Medicine, Pittsburgh, Pennsylvania, U.S.A.

[3]University of Pittsburgh Cancer Institute Brain Tumor Center, Pittsburgh, Pennsylvania, U.S.A.

[4]Texas Children's Hospital, Baylor College of Medicine, Pittsburgh, Pennsylvania, U.S.A.

[5]University of Pittsburgh Molecular Biology Information Service, Pittsburgh, Pennsylvania, U.S.A.

[6]University of Pittsburgh Cancer Institute, Pittsburgh, Pennsylvania, U.S.A.

[7]University of Pittsburgh Drug Discovery Institute, Pittsburgh, Pennsylvania, U.S.A.

[8]Department of Computational and Systems Biology, University of Pittsburgh School of Medicine, Pittsburgh, Pennsylvania, U.S.A.

[#] These authors contributed equally to this work.

Abstract

To improve therapeutic responses in glioma patients, new combination therapies that exploit a mechanistic understanding of the inevitable emergence of drug resistance are needed. Intra-tumoral heterogeneity enables a low barrier to resistance in individual glioma patients. We reasoned that targeting two or more fundamental processes that gliomas are particularly dependent upon could result in pleiotropic effects that would reduce the diversity of resistant subpopulations allowing convergence to a more robust therapeutic strategy. In contrast to the cytostatic responses

Address correspondence to: Dr. Ian F. Pollack, Chief, Pediatric Neurosurgery, Children's Hospital of Pittsburgh, Department of Neurological Surgery, University of Pittsburgh School of Medicine, 530 45th St. Pittsburgh, PA, 15201, U.S.A. Phone: 412-692-5881; ian.pollack@chp.edu or Dr. Daniel R. Premkumar, Department of Neurological Surgery, University of Pittsburgh School of Medicine, 530 45th St. Pittsburgh, PA, 15201, U.S.A. Phone: 412-692-9233; daniel.premkumar@chp.edu.

Authors' Contributions

Conception and design: Ian F. Pollack and Andrew M. Stern

Development of methodology: Esther P. Jane, Daniel R. Premkumar and Sameer Agnihotri

Acquisition of data (provided animals, acquired and managed patients, provided facilities etc.): Esther P. Jane, Daniel R. Premkumar, Swetha Thambireddy, Brian Golbourn, Sameer Agnihotri, Kelsey C. Bertrand, Stephen C. Mack, Sameer Agnihotri, Max I. Myers, and Ansuman Chattopadhyay

Analysis and interpretation of data (e.g., statistical analysis, biostatistics, computational analysis): Esther P. Jane, Daniel. Premkumar, Brian Golbourn, Sameer Agnihotri, Kelsey C. Bertrand, Stephen C. Mack, Sameer Agnihotri, and Mark Schurdak

Writing, review, and/or revision of the manuscript: Daniel R. Premkumar, Sameer Agnihotri, Lansing Taylor, Mark Schurdak, Andrew Stern and Ian F. Pollack. All the authors edited and approved the manuscript.

Disclosure of Potential Conflict of Interest

The authors have declared that no conflict of interest exists.

Author Manuscript Author Manuscript Author Manuscript Author Manuscript

observed with each drug alone, the combination of the HDAC inhibitor panobinostat and the proteasome inhibitor bortezomib synergistically induced apoptosis of adult and pediatric glioma cell lines at clinically achievable doses. Resistance that developed was examined using RNA sequencing and pharmacological screening of resistant versus drug naive cells. Quinolinic acid phosphoribosyltransferase (QPRT), the rate-determining enzyme for de novo synthesis of nicotinamide adenine dinucleotide (NAD+) from tryptophan, exhibited particularly high differential gene expression in resistant U87 cells and protein expression in all resistant lines tested. Reducing QPRT expression reversed resistance, suggesting that QPRT is a selective and targetable dependency for the panobinostat-bortezomib resistance phenotype. Pharmacological inhibition of either NAD+ biosynthesis or processes such as DNA repair that consume NAD+ or their simultaneous inhibition with drug combinations, specifically enhanced apoptosis in treatment-resistant cells. Concomitantly, de novo vulnerabilities to known drugs were observed.

Keywords

Panobinostat; bortezomib; synergy; resistance; glioma; quinolate phosphoribosyltransferase

Introduction

Malignant gliomas are the most common, highly infiltrative, rapidly growing tumors of the central nervous system (CNS) in both children and adults. Recent studies have demonstrated the existence of multiple tumor subgroups within the broad category of high-grade gliomas, which differ in terms of their molecular characteristics and demographic features. Diffuse midline gliomas (DMGs) such as diffuse intrinsic pontine glioma (DIPG) are universally lethal central nervous system (CNS) tumors, have a particularly poor prognosis, with one-year progression-free survival less than 20%, which may in part reflect its infiltrative phenotype and location. Surgical removal of DIPGs is almost always not possible. Therefore, treatment strategies have traditionally been limited to radiotherapy and chemotherapy. Outcomes are marginally better, but still poor, for lesions arising outside the brainstem in both children and adults, where the one-year progression-free survival rates are approximately 40% (1–5). Accordingly, novel treatment approaches are required to improve the dismal prognosis of patients with these tumors.

Extensive inter-tumoral and intra-tumoral heterogeneity are features of gliomas with the latter enabling a low barrier to treatment resistance in individual patients (6). To achieve more durable responses, we reasoned that targeting two or more fundamental processes that gliomas are particularly dependent upon could result in pleiotropic effects that would reduce the diversity of resistant subpopulations thereby enabling convergence to a more robust therapeutic strategy. Along these lines, recent phase I and II studies by McCracken et al (7) demonstrated a modest survival benefit with temozolomide in combination with the angiogenesis inhibitor bevacizumab and the proteasome inhibitor bortezomib for recurrent glioma. Grasso et al screened 83 targeted inhibitors in a panel of patient-derived DIPG cell lines. Their study revealed that the HDAC inhibitor panobinostat had strong therapeutic efficacy in vitro and in DIPG orthotopic xenograft models (5). Complementary to these studies, we previously demonstrated that the combination of an HDAC inhibitor, vorinostat,

Author Manuscript Author Manuscript Author Manuscript Author Manuscript

with a proteasome inhibitor, bortezomib, produced synergistic augmentation of glioma cell killing *in vitro* (8) and was the most effective combination among many tested, making a HDAC/proteasome inhibitor combination a promising strategy for further examination.

Herein we demonstrate that the combination of panobinostat and bortezomib was particularly effective in synergistically killing glioma cells derived from all high-grade human adult and pediatric glioma cell lines tested while sparing non-neoplastic human astrocytes. After a 30-day treatment, cell populations resistant to the panobinostat-bortezomib combination did emerge. Differential gene expression analysis was performed to identify gene(s) or pathway(s) that could account for this acquired resistance and identified quinolinic acid phosphoribosyltransferase (QPRT) as highly upregulated in cells treated with the inhibitors. This enzyme (QPRT) converts quinolinic acid (QA) to nicotinamide mononucleotide (NAMN), a precursor of the ubiquitous coenzyme nicotinamide adenine dinucleotide (NAD), via transfer of a phosphoribosyl moiety from 5-phospho-d-ribose-1-diphosphate (PRPP) in one of the rate determining steps for de novo NAD+ biosynthesis from tryptophan (9, 10). In conjunction with RNAi and small molecule inhibition studies, we demonstrated an exquisite dependence of the resistant cells on NAD+ biosynthesis and its utilization in comparison to the drug naïve cells. Indicative of the significant changes in cell regulation required to resist the panobinostat-bortezomib combination, de novo vulnerabilities of the resistant glioma cells to 5-fluorouracil and gemcitabine in comparison to the drug naïve cells also emerged. The sensitivity across diverse glioma cell lines to panobinostat-bortezomib and the selective de novo vulnerabilities of the resistant population to inhibition of NAD+ biosynthesis and to known drugs inform strategies for treating both adult and pediatric high-grade gliomas.

Materials and Methods

Reagents

Panobinostat, vorinostat, pracinostat, trichostatin-A (TSA), RG2833, entinostat, bortezomib, marizomib, FK866, niraparib, selisistat, gefitinib, enzastaurin, dasatinib, dinaciclib, PI103, PD-0325901, HSP990, ABT737, (+)- JQ, TP0903, Bay11–7082, YM155, and cucurbitacin-I were purchased from Selleck Chemicals (Houston, TX). Vincristine, vinblastine, paclitaxel, topotecan, gemcitabine, 5-fluoruracil, and temozolomide were purchased from Sigma Aldrich (St. Louis, MO).

Cell lines

U87 and A172 human glioma cell lines were obtained from American Type Culture Collection (Manassas, VA, USA). LN18, LNZ308 were provided by Dr. Nicolas de Tribolet (Lausanne, Switzerland). SJG 2 cell line was a kind gift from Dr. Chris Jones at the Institute of Cancer Research, London, England. Cell culture conditions of these cell lines were as previously described (11). The HSJD-DIPG-007 (referred to as DIPG 007 in the manuscript) cell line was kindly provided by Dr. Montero Carcaboso (Hospital San Joan de Déu, Barcelona, Spain) and cultured as reported previously (5, 12). GIBCO® Human Astrocytes, were purchased from Gibco Life Technologies and cultured using GIBCO® Astrocyte Medium (Thermo Fisher Scientific, Pittsburgh, PA). Morphological changes in response to

Author Manuscript Author Manuscript Author Manuscript Author Manuscript

inhibitor treatment were evaluated periodically by microscopic (EVOS, Thermo Fisher Scientific, Pittsburgh, PA) inspection. Cell lines used in this study (U87, A172, LN18 and LNZ308) were authenticated using Short Tandem Repeat (STR) analysis by ATCC cell line authentication service (Manassas, VA). Samples were processed using the ABI Prism® 3500xl Genetic Analyzer and data was analyzed using GeneMapper® ID-X v1.2 software (Applied Biosystems). The genetic profiles for the samples were identical to the reported profile. Other cell lines (SJG 2, DIPG 007 and human astrocytes) were not authenticated. No mycoplasma testing regimen was performed.

Cell viability assay

U87, A172, LN18, LNZ308 and SJG 2 cells (3 × 103/well) were plated in 96-well microtiter plates (Costar, Cambridge, MA) in 75μl of growth medium overnight. DIPG 007 neurospheres were dissociated by incubation in Accutase (Thermo Fisher, Waltham, MA, USA) for 5 min at 37°C. After a mild mechanical dissociation by pipetting, cells were filtered through a 100 μm cell strainer to generate a single-cell suspension. Cells were centrifuged at 200g for 5 min, counted and seeded at 3000 cells/well in 96-well plates. On the following day, an equal volume of inhibitors (at 2X concentration) was added to each well using a multichannel pipette. Control cells received an equivalent amount of DMSO (vehicle). Inhibitor dilution series were added in quadruplicate. In parallel, replicates of 150 μl of media without cells served as the blanks. After 72 h of incubation at 37°C, the number of viable cells was determined using a colorimetric cell proliferation assay kit (CellTiter96 Aqueous Non-Radioactive Cell Proliferation Assay; Promega, Madison, WI), as reported previously (13). All experiments (in 4 wells) were performed at least three times. The inhibitor concentrations required to inhibit cell growth by 50% (IC50) were calculated by plotting the percent inhibition of proliferation in inhibitor-treated cells compared to vehicle-treated cells (Y-axis) versus the log of the concentration of drug (X-axis) using 4-parameter logistic fit using GraphPad Prism 6.0 software, (San Diego, CA).

Annexin V and propidium iodide apoptosis assay

Apoptosis induction in vehicle- or inhibitor-treated cells was assayed by the detection of membrane externalization of phosphatidylserine using an Annexin V assay kit (Invitrogen) as described previously (13). 2×10^5 cells were harvested at various intervals after treatment, washed with ice-cold phosphate-buffered saline (PBS) and resuspended in 200 μl of binding buffer. Annexin V-FITC and 1 μg/ml propidium iodide were added and cells were incubated for 15 min in a dark environment. Labeled cells were analyzed by flow cytometry (Becton Dickinson-LSRII, BD Biosciences).

Generation of inhibitor-resistant cell lines

To address whether cotreatment of HDAC and proteasome inhibitors generate resistance, cells were treated with single agent or the combination of both for 72 h (panobinostat at 2.5 nmol/L and bortezomib at 0.25 nmol/L respectively -starting with a dose that was approximately 10% of the clinically relevant concentration, Supplemental Figure 1). Control cells received an equal amount of vehicle (DMSO). Viable cells after vehicle- or inhibitor-treatment were isolated using a BD ARIAII cell sorter (BD Biosciences, San Jose, CA). Live cells (annexin and PI negative) were then isolated, washed with Hank's Balanced Salt

Author Manuscript Author Manuscript Author Manuscript Author Manuscript

Solution (HBSS, Invitrogen) and cultured in growth media containing double the concentration of inhibitor(s). Once surviving cells reached 60–80% confluency, this process was repeated until the resulting cell populations were resistant to the clinically relevant concentration (panobinostat, 25 nmol/L and bortezomib, 2.5 nmol/L). These resistant cells were given an interval to "*recover*" from therapy, by culturing in inhibitor-free complete medium for an additional 30 days before using for comparison. During the 30-day recovery period, cells were trypsinized at 72-hour intervals and fresh media was added to ensure inhibitors had been thoroughly removed. The flasks with all cell types were incubated at 37°C in an atmosphere of 5% CO2 and 95% humidity.

Cell cycle analysis

The effect of varying concentrations of inhibitors on cell cycle distribution was determined as described previously (11). Cells treated with inhibitors or vehicle were collected and fixed with 80% ethanol on ice for 30 min, then washed with HBSS. After being resuspended in HBSS with 50 μg/mL RNase and 50 μg/mL propidium iodide, cell cycle distributions were analyzed using a Becton Dickinson-LSRII flow cytometer (Beckman Coulter). The percentages of cell populations in each cell cycle phase (sub-G1, G1, S, G2-M) were calculated from DNA content histograms using Cell Quest software (Becton Dickinson Immunocytometry, San Jose, CA).

Western blotting analysis

Cells were washed in cold PBS and lysed in buffer containing 30 mM HEPES, 10% glycerol, 1% Triton X-100, 100 mmol/L NaCl, 10 mmol/L $MgCl_2$, 5 mM EDTA, 2mM Na_3VO_4, 2 mM β-glycerophosphate, 1 mM phenylmethylsulfonyl fluoride, 1 mmol/L 4-(2-aminoethyl) benzenesulfonyl fluoride, 0.8 μmol/L aprotinin, 50 μmol/L bestatin, 15 μmol/L E-64, 20 μmol/L leupeptin, and 10 μmol/L pepstatin A for 15 min on ice. Samples were centrifuged at 12,000g for 15 min, supernatants were isolated, and protein was quantified using Protein Assay Reagent (Pierce Chemical, Rockford, IL). Equal amounts of protein were separated by SDS polyacrylamide gel electrophoresis (PAGE) followed by Western blot analysis as described previously (11). The following antibodies used: cleaved caspase-3 (#9664), and cleaved PARP (#9546), were from Cell Signaling Technology (Beverly, MA). QPRT (MA5–25200) was from Thermo Fisher Scientific (Rockford, IL), respectively. β-actin (#3700, Cell Signaling Technology) antibody was used to ensure equal loading and transfer of proteins.

DiOC6 labeling and detection of mitochondrial membrane depolarization

Mitochondrial membrane depolarization was measured as described previously (11). In brief, floating cells were collected, and attached cells were trypsinized and resuspended in PBS. Cells were loaded with 50 nmol/L 3',3'-dihexyloxacarbo-cyanine iodide (DiOC6, Molecular Probes, Invitrogen) at 37°C for 15 min. The positively charged DiOC6 accumulates in intact mitochondria, whereas mitochondria with depolarized membranes accumulate less DiOC6. Cells were spun at 3,000 × g and rinsed with PBS twice and resuspended in 1 ml of PBS. Following acquisition of data (CellQuest software (Becton Dickinson), the cell fluorescence information was saved in the Flow Cytometry Standard (.fcs) format. These files were then accessed with the FlowJo analysis software (Tree Star,

Author Manuscript Author Manuscript Author Manuscript Author Manuscript

Inc., Ashland, OR). Through this software, the fluorescence data were plotted as histograms, which were converted into and saved as Scalable Vector Graphics (.svg) files. Using Inkscape (The Inkscape Team), an Open Source vector graphics editor, the data were compiled into two-dimensional histogram overlays for comparative analysis. The loss of mitochondrial membrane potential was quantified in FlowJo by gating any left-shifted populations and subtracting from control, and the percentage of cells with decreased fluorescence was determined.

Transient transfection

Cells were transiently transfected according to the manufacturer's protocol (Dharmacon, Lafayette, CO). Briefly, cells were seeded in 6-well tissue culture plates (Costar, Cambridge, MA) at a density of 2×10^5 per well. After overnight attachment period, just prior to transfection, the culture medium was removed and replaced with 1ml of OPTI-MEM I (Gibco, Carlsbad, CA). Cells were then transfected with 200 nmol/L siRNA using DharmaFECT transfection reagent to deliver siRNA. Four sequence-specific commercially available ON-TARGET-plus siRNA for human QPRT (QPRT-1, catalog number J-003989-09-0002; QPRT-2, catalog number J- 003989-10-0002; QPRT-3, catalog number J-003989-11-0002 and QPRT-4, catalog number J- 003989-12-0002) and non-target control siRNA (catalog number D-001830-01-05) sequences were used for this study (Dharmacon). After 8 h of transfection, OPTI-MEM I medium was replaced with 3 ml growth medium. After 72 h of post-transfection, the cells were subjected to western blot assay (to verify transfection efficiency) and for apoptosis analysis. Because DIPG cells are impervious to the introduction of siRNA using standard laboratory techniques (14), we used U87 and SJG 2 cell lines for this study.

RNA sequencing, differential data analysis and gene enrichment analysis

Cells were trypsinized, lifted and total RNA was extracted using Qiagen RNeasy Mini Kit according to the manufacturer's recommendation (Qiagen Sciences Inc., Germantown, MD). Triplicate samples were made for every culture condition. The quantity and purity of the RNA was determined by absorbance at 260 nm and by 260/280 absorbance ratio, respectively. RNA sequencing was performed by Novogene (Sacramento, CA). After quality assessment and preprocessing the raw sequencing reads (paired end read, 2 × 100 base pairs), were aligned to human reference genome. Differential expression analysis was done with a fold change of ±1.5 and $*P < 0.05$. For gene-ontology "GO" analysis we used we used the publicly available GO module implemented by the Gene Set Enrichment Analysis (GSEA) data portal hosted at the Broad Institute, Cambridge, MA (http://software.broadinstitute.org/gsea/index.jsp).

NAD+ quantification

Total intracellular NAD+ content was measured using the colorimetric assay kit (Sigma, MO, USA, Catalog number MAK-037). Briefly, 1×10^5 cells were seeded in 6-well plates. After overnight incubation at 37°C, the cells were treated with inhibitors for the indicated duration. Cells were harvested, by centrifugation at 12,000 rpm at 4°C for 20 minutes, and the total NAD+ was determined, according to the manufacturer's instructions. Briefly, cells were lysed by lysis buffer (provided in the kit) and the lysate was deproteinized using

Author Manuscript Author Manuscript Author Manuscript Author Manuscript

deproteinizing sample preparation kit (Abcam, catalog number 204708) to avoid enzymatic digestion. Protein concentration was determined using a BCA protein assay kit (Pierce, Rockford, IL, USA). Equal amount of protein was taken, subsequently, the lysate was incubated with enzyme mix and the developer solution (provided in the kit) in 96-well plates in triplicate. The plate was incubated at room temperature for 30 min in the dark and absorbance was measured at 450 nm by BioTek, Synergy HTX multimode plate reader (Winooski, VT, USA).

Statistical analysis

Unless otherwise stated, data are expressed as mean ± S.D. Statistical analyses were conducted using Prism 6.0 GraphPad software. ANOVA analysis was conducted for multigroup comparisons followed by a post-hoc Dunnett's test (groups compared with one control group) or post-hoc Tukey's test (to identify differences among subgroups). Where appropriate, direct comparisons were conducted using an unpaired two-tailed Student t test. Statistical significance was established for $P < 0.05$.

Results

HDAC and proteasomal inhibitors reduced human glioma cell growth in vitro

Our initial focus was to identify potent HDAC and proteasome inhibitors that effectively blocked the growth of a diverse panel of glioma cell lines. First, we examined a set of six HDAC inhibitors in adult (U87, A172, LNZ308, and LN18) and pediatric (SJG 2) high-grade glioma and pediatric brain stem glioma (DIPG 007) cell lines for their effect on cell proliferation using the MTS assay. As a single agent, panobinostat, vorinostat, pracinostat, entinostat and trichostatin A in contrast to RG2833 inhibited cell proliferation in a concentration-dependent manner (Fig. 1A). Examination of dose-response curves and their IC50 values revealed that there were considerable differences in potency and maximal extent of growth inhibition among each of the HDAC inhibitors and across the cell lines. Panobinostat was consistently the most efficacious inhibitor across all cell lines tested inhibiting the proliferation of both pediatric and adult glioma cells, with IC50 values in the low nanomolar range (U87, 0.105 μmol/L; LNZ308, 0.086 μmol/L; A172, 0.079 μmol/L; LN18, 0.118 μmol/L; SJG 2, 0.033 μmol/L; and DIPG 007, 0.026 μmol/L) and was the HDAC inhibitor selected for subsequent studies. Interestingly, although RG2833 is a highly potent and brain penetrant HDAC inhibitor (15), it exhibited relatively poor efficacy. This observation was not necessarily expected but may relate to the apparent requirement of a pan-HDAC inhibitor profile intrinsic to panobinostat in contrast to RG2833 that is selective for inhibiting only class 1 HDACs. In support of this hypothesis, entinostat, the other class 1 selective HDAC inhibitor tested also displayed relatively weak efficacy compared to the other nonselective HDAC inhibitors.

As a prospective complement to panobinostat-based combination therapy we next examined the effects of two proteasome inhibitors as single agents on cell proliferation, the boronic acid-based bortezomib and the marine natural product marizomib. As indicated (Fig. 1B), both proteasome inhibitors effectively blocked cell growth of all six glioma lines tested in

Author Manuscript Author Manuscript Author Manuscript Author Manuscript

the low nanomolar range with bortezomib consistently showing 10-fold greater potency than marizomib.

Cotreatment with bortezomib enhances the efficacy of Panobinostat

Although the combination of HDAC and proteasomal inhibitors have been extensively studied in adult glioma (8, 16–19), information on pediatric gliomas has been limited. First, we examined whether treatment with panobinostat or bortezomib or their combination substantially impacted cell viability. Staining with FITC-labeled annexin V and propidium iodide revealed that clinically relevant doses of panobinostat or bortezomib each led to a minimal or modest cell death. However, the combination of panobinostat and bortezomib significantly enhanced cell death in both adult and pediatric glioma cell lines (Fig. 2A). Western blot analysis showed that cotreatment with panobinostat and bortezomib increased caspase 3 and PARP cleavage, which is the hallmark feature of caspase -dependent apoptosis (Fig. 2B). In contrast, when examined with non-neoplastic human astrocytes, we noted that cotreatment with panobinostat and bortezomib at clinically relevant concentrations did not induce apoptosis, suggesting selectivity towards tumor cells (Fig. 2C).

Acquired resistance to panobinostat and bortezomib

Despite the substantial induction of apoptosis by the panobinostat-bortezomib combination in all six cell lines tested, 100% apoptosis was not evident for any one cell line (Fig. 2A). This observation raised the possibility that subpopulations of glioma cell lines resistant to the combination may exist. To address whether cells treated with the combination of panobinostat and bortezomib would acquire resistance, we exposed U87, SJG 2 and DIPG 007 to physiologically relevant drug concentrations for several weeks using repeated cycles of inhibitor selection (Supplemental Figure 1). We did not observe any discernable differences in the morphology (Fig. 3A) and cell viability (Fig. 3B) between the corresponding vehicle-treated (drug naïve) cells versus the long-term inhibitor-treated cells for each glioma cell line studied. To examine whether inhibitor-treated cells (U87, SJG 2 and DIPG 007 cell populations) differ substantially from naïve cells in their cytotoxic response to fresh administration of drugs, drug naïve and previously treated cells were exposed to panobinostat-bortezomib combination for 72 hours and then analyzed for apoptosis using Annexin V and propidium iodide staining. As shown in Fig. 3B, exposure of previously treated and selected U87, SJG 2 and DIPG 007 cells (Supplemental Figure 1), to physiologically relevant concentrations of the panobinostat-bortezomib combination induced minimal toxicity (i.e., < 10% apoptosis) that was indistinguishable from vehicle alone. In contrast, when the drug naïve cells were treated with the panobinostat-bortezomib combination, 80 % apoptosis was observed. The results of this study were quantitatively mirrored using alternative indicators of apoptosis that included loss of mitochondrial membrane potential (Supplemental Figure 2) and the accumulation of cells in a subG1 phase of the cell cycle (Supplementary Figure 3). These findings raise the possibility that in glioma cells, sustained exposure to panobinostat and bortezomib appears to provoke a high degree of resistance.

Author Manuscript Author Manuscript Author Manuscript Author Manuscript

RNA-sequencing identifies quinolinic acid phosphoribosyltransferase (QPRT) as a highly expressed gene in bortezomib-panobinostat resistant U87 cells.

To identify potential genes and gene-expression patterns that may contribute to resistance, we initially performed RNA-sequencing analysis using the U87 cell line. Biological triplicates of control (drug naïve), bortezomib-resistant, panobinostat-resistant, bortezomib and panobinostat-resistant (cotreatment with both bortezomib and panobinostat) cells, and "*recovery*" cells (where drug was removed after resistance was generated to dual inhibitors, and the cells were cultured for an additional 30 days in inhibitor-free medium) were used. Hierarchical clustering of the top 1000 most variable genes robustly separated all control and treatment groups (Fig. 4A). Next, we compared drug naïve control cells to (i) bortezomib resistant cells, (ii) panobinostat resistant cells, (iii) dual resistant cells, and (iv) recovery cells to identify differentially expressed transcripts. Differential genes were identified using a Wilcoxon rank-sum test with a minimum of 1.5-fold change, a p-value of $p<0.05$ and a false discovery rate of $q<0.10$. Differentially expressed genes are listed in Supplemental File 1. We identified 516 differentially expressed genes comparing control to bortezomib resistant cells (Supplemental Fig. 4A), 343 differentially expressed genes comparing control to panobinostat resistant cells (Supplemental Figure. 4B), 695 genes comparing control to dual drug resistant cells (Supplemental Figure. 4C) and 569 genes comparing control to our recovered cells (Supplemental Figure. 4D). Interestingly, we identified 47 genes common to all resistant to control comparisons (Fig. 4B), including QPRT, CHI3L1, BOC, IGFN1, HLA-DQB1, ITGAX and ADCY8 (Fig. 4C and Supplemental File 2). We hypothesized that these genes may represent a general mechanism of drug resistance. A statistical Overrepresentation Test using Protein ANalysis THrough Evolutionary Relationships classification (PANTHER) analysis identified several significant signaling pathways from each of our experimental conditions (Supplemental File 3). Moreover, the persistence of select genes even after drug removal may represent newly acquired dependencies selective for the resistant cell state that may create new therapeutic vulnerabilities. Also, a significant enrichment emerged in genes belonging to extracellular matrix organization, extracellular structure organization, response to organic substance, response to cytokine, cellular response to chemical stimulus, cytokine-mediated signaling pathway, cell adhesion, regulation of cell migration and interferon-gamma-mediated signaling pathway (Supplemental File 3).

QPRT, an enzyme catalyzing the rate-determining conversion of quinolinic acid (QA) to nicotinic acid mononucleotide (NAMN) a precursor for de novo NAD+ biosynthesis from tryptophan (20) (Fig. 4D), was the gene that had the highest degree of differential expression, with a >10-fold increase in resistant versus naïve U87 cells (Fig. 4C and Supplemental File 3). Analysis of RNA expression from the TCGA database (21–26) indicated that QPRT was overexpressed in both adult and pediatric glioma relative to normal brain tissue (Fig. 4E–G). Although our analysis did not show a significant correlation of QPRT expression with survival (Fig. 4H), in recurrent glioblastoma after radio-chemotherapy QPRT expression was associated with a poor prognosis in two independent data sets (27). Therefore, based on these analyses that suggest potential clinical relevance particularly for therapy resistance, our initial studies focused on QPRT.

Author Manuscript Author Manuscript Author Manuscript Author Manuscript

Targeting QPRT decreases survival of the resistant cells

The striking increase in QPRT RNA expression was validated at the protein level in inhibitor-resistant (Fig. 5A) and “recovery” cells (Fig. 5B) with minimal detectable protein observed in drug naïve control cells. Importantly, recovery cells resulted in a decreased level of QPRT protein relative to resistant cells, which was associated with a statistically significant increase in the induction of apoptosis following panobinostat and bortezomib treatment, suggesting that relatively high levels of QPRT may confer a mechanism of prolonged resistance after drug exposure that wanes slowly over time (Fig. 5C, left panel). To elucidate the biological significance of QPRT, we first compared the NAD+ levels of naïve versus inhibitor-resistant cells hypothesizing that the increased levels of QPRT could enhance overall de novo NAD+ biosynthesis. A 4–7-fold elevation of NAD+ levels was observed in resistant U87 cells treated with panobinostat or bortezomib or their combination (Fig. 5D, left panel), raising the possibility that resistant cells efficiently replenish and/or supply NAD+ to provide a survival advantage over drug naïve counterparts. We then examined the potential functional association of increased QPRT levels to the resistant phenotype in U87 cells, by employing an RNA interference approach. Seventy hours after transfection, the knockdown efficacy of four QPRT siRNAs was semi-quantitated by Western blot analysis. As shown in Fig. 5E, QPRT siRNA 1 and 2 suppressed the expression of QPRT protein levels significantly (>75%) when compared to QPRT siRNA 3 and 4. Western blot (Fig. 5F) and cell viability analysis (Fig. 5G) assay revealed that silencing QPRT (with QPRT siRNA-1) significantly increased apoptosis. Similar results were found with QPRT siRNA 2 (Supplemental Fig. 5), suggesting that QPRT may be a potential target to sensitize resistant cells and may be required to confer at least partial resistance to panobinostat + bortezomib treatment.

Targeting NAD+ biosynthesis pathway overcomes panobinostat and bortezomib-induced resistance

In addition to de novo biosynthesis from tryptophan with QPRT catalyzing the rate limiting step, NAD+ is mainly produced via salvage synthesis pathways, whereby nicotinamide phosphoribosyltransferase (NAMPT) constitutes the rate-limiting step in nicotinamide-dependent salvage (refer Fig. 4D) (28). Given the selective dependency of panobinostat-bortezomib resistant cell viability on QPRT and the elevated level of NAD+ in the resistant cells relative to their drug naïve counterpart we reasoned that these cells would also be dependent on NAMPT activity. To further address the impact of interfering with NAD+ biosynthesis on inhibitor-resistant cells, we examined the effects of a selective NAMPT inhibitor FK866. U87 cells were incubated with FK866 or vehicle (DMSO) and intracellular NAD+ content and cell viability was assessed after 72 h. In comparison to untreated cells, a significant reduction of the intracellular amount of NAD+ (between 75–90%) was observed in FK866-treated cells (Fig. 6A, left panel). Furthermore, FK866 effectively and selectively induced apoptosis in drug-resistant or “recovery” cells compared to naïve cells (Fig. 6B, left panel). In drug naive cells, minimal number of the cells are double positive for PI and Annexin V after treatment with FK866 for 72 hours. However, apoptotic cell death was more profound in panobinostat and bortezomib-resistant cells, highlighting the exquisite dependency of the resistant cells on NAD+ biosynthesis. A similar effect was seen in the “recovery” cells that retained relatively high levels of QPRT (Fig. 5B). Therefore, we

Author Manuscript Author Manuscript Author Manuscript Author Manuscript

reasoned that in comparison to naïve cells the panobinostat and bortezomib resistant cells would also be dependent on processes that consumed NAD+. In support of this hypothesis we observed that inhibition of the NAD+ consuming enzymes PARP1 and Sirtuin by niraparib (Fig. 6C, left panel) and selisistat (Fig. 6D, left panel) respectively as single agents produced an increased fraction of apoptotic cell death in panobinostat plus bortezomib resistant and recovery cells compared to drug naïve U87 cells. Strikingly, when U87 cells were treated with each of these inhibitors in the presence of FK866, we observed a significant increase in cell death (to approximately 60–90%) that was specific to the resistant cells. This sensitizing effect of FK866 on niraparib (Fig. 6E, left panel) and selisistat-induced (Fig. 6F, left panel) cytotoxicity was observed in both resistant and recovery cells, suggesting that targeting NAD+ biosynthesis pathway or the enzymes consuming NAD+ could be a rational strategy to sensitize panobinostat and bortezomib-resistant U87 cells.

Given the large changes in global gene expression that accompanied panobinostat and bortezomib resistance in glioma, we determined if resistance was associated with de novo vulnerabilities that were either distinct from or indirectly related to NAD+ biosynthesis and consumption. Therefore, we applied a chemogenomics approach connecting a particular cell state (ie. resistance) to drug-mode-of-action (29) and assembled a panel of inhibitors to represent a spectrum of known mechanisms that might promote apoptosis, including a receptor kinase inhibitor (gefitinib), PKC inhibitor (enzastaurin), Src family kinase inhibitor (dasatinib), CDK inhibitor (dinaciclib), PI3K/Akt/mTOR pathway inhibitor (PI-103), MAP kinase inhibitor (PD 0325901), heat shock protein inhibitor (NVP-HSP990), Bcl-2/Bcl-xL inhibitor (ABT 737), bromodomain and extra terminal domain (BET) protein inhibitor (JQ1), AXL Inhibitor (TP 0903), NF-κB inhibitor (Bay 11–7082), survivin inhibitor (YM 155), JAK/STAT inhibitor (cucurbitacin I), and chemotherapeutic agents (inhibitors disrupting microtubule dynamics, vincristine, vinblastine and taxol); topoisomerase inhibitor, topotecan; alkylating agent, temozolomide; deoxycytidine analogue and nucleic acid synthesis inhibitor, gemcitabine; an analog of the nucleoside pyrimidine, 5-fluorouracil). For most agents, we did not observe a difference in apoptosis induction between drug naïve and drug-resistant U87 cells (Supplemental Fig. 6A). However, administration of gemcitabine or 5-fluorouracil significantly increased apoptosis in resistant cells compared to drug naïve cells, suggesting that these nucleoside analogs may provide complementary opportunities for therapeutic interventions to overcome panobinostat and bortezomib-induced resistance in glioma (Supplemental Fig. 6A and B).

Resistant pediatric glioma cells exhibit an NAD+ biosynthesis dependency

We next determined if the NAD+ biosynthetic dependency evident for the adult glioma U87 cell line was also a phenotype exhibited by the pediatric glioma cells lines, SJG2 and DIPG-007. Comparative RNAseq analysis among the three cell lines showed very little overlap of naïve versus resistant cells gene expression patterns (Supplemental File 4). In contrast to the 10-fold increase in QPRT gene expression at the RNA level observed for resistant U87 cells, SJG2 cells showed a modest but significant 1.4-fold increase ($p=0.048$, Supplemental File 5 and Supplemental Fig.7). The increase in QPRT expression at the protein level in the SJG 2 resistant cells was comparable to this increase observed in the U87 resistant cells (Fig. 5A and Fig. 5B) Consistent with this observation, the phenotypes of the

Author Manuscript Author Manuscript Author Manuscript Author Manuscript

SJG 2 and U87 cells as determined by biochemical (Fig. 5A and Fig. 5B, QPRT protein expression) pharmacological (Fig. 5D and Fig. 6A, NAD+ content), and knockdown studies (Fig. 5E–G and Supplemental Fig. 5) were strikingly similar and indicative of a selective NAD+ biosynthesis dependency for the panobinostat + bortezomib resistant cells. The most significant difference between these two cell lines (U87 and SJG 2) was the increased sensitivity of the SJG 2 cells to the NAD+ salvage biosynthesis pathway inhibitor, FK866 (compare Fig. 6B, left versus middle panel). Consequently, the selectivity of FK866 for resistant cells in comparison to their naïve counterpart was diminished at higher concentrations of the drug for the SJG 2 cells relative to the U87 cells.

The DIPG 007 cells exhibited no significant difference for QPRT gene expression at the RNA level between naïve and drug resistant cells (Supplemental File 4 and 5 and Supplemental Fig. 7). However, the absolute level of QPRT expression in the naïve DIPG 007 cells was 8-fold higher than the level in naïve U87 cells and comparable to the increased level seen in the drug resistant U87 cells (Supplemental File 5 and Supplemental Fig. 7). Increased QPRT protein expression in the resistant DIPG-007 cells relative to their drug naïve counterparts as observed for the U87 and SJG 2 cell lines was also evident (Fig. 5A and Fig. 5B). In contrast to the U87 and SJG2 cell lines, we identified nicotinamide N-methyltransferase (NNMT) upregulated in the drug resistant DIPG-007 cell line in comparison to the corresponding drug naïve cells (5.7-fold increase, $p < 1.70E-04$; Supplemental File 4; see Discussion). The NAD+ levels in the drug resistant DIPG 007 were elevated compared to the naïve DIPG 007 cells as similarly observed for the U87 and SJG2 cell lines (Fig. 5D). The overall pharmacological profile for the naïve and drug resistant DIPG 007 cells was similar to the other two (U87 and SJG 2) cell lines (Fig. 5A and Fig. 5B, QPRT protein expression; Fig. 5D, NAD+ content). However, the differential sensitivity between the resistant and naïve cells to the pharmacologic agents tested was not as large as observed for the other two cell lines (Fig. 6B, FK866; Fig. 6C, niraparib; Fig. 6D, selisistat).

Discussion

The observation that the combination of panobinostat and bortezomib was effective in synergistically killing glioma cells derived from all high-grade human adult and pediatric glioma cell lines tested while sparing non-neoplastic human astrocytes is consistent with our previous studies (8) and others that are providing the rationale for clinical trials to address this devastating disease (7, 18, 19, 30, 31). Addressing the emergence of resistance to therapy for glioma is often limited by suboptimal pharmacodynamic effects caused by inefficient blood-brain barrier penetrance. Technical advancements for improving the blood-brain barrier penetrance of these drugs and the development of newer members within these two drug classes having more optimal pharmaceutical properties are expected to support further development of proteasome-HDAC inhibitor combinations for glioma (32–38). For example, marizomib would be preferred over bortezomib for our planned *in vivo* studies because of its superior blood-brain barrier penetrance (31, 32).

Additionally, we reasoned that blocking two fundamental processes such as proteostasis and histone deacetylation that gliomas are particularly dependent upon could result in pleiotropic effects that would reduce the diversity of resistant populations (39–41). Nevertheless, despite

Author Manuscript Author Manuscript Author Manuscript Author Manuscript

the synergism we observed, there was not 100% cell killing suggesting that even in the case of cell lines the hallmark intra-tumoral heterogeneity of gliomas might present a low barrier to the selection of resistant subpopulations. Therefore, this study focused on the identification and characterization of resistance to the panobinostat-bortezomib combination with the goal of leveraging the mechanistic insights gained to optimize therapeutic strategies involving this promising combination for glioma.

Using a dose escalation protocol for three cell lines, adult (U87), pediatric (SJG 2) high-grade glioma, and pediatric brain stem glioma (DIPG 007) we were able to select for resistance to all three cell lines at clinically achievable drug concentrations. Interestingly, these resistant populations were indistinguishable from their drug-naïve counterparts with respect to morphology and cell cycle profile. Conducting RNA Seq analyses in the U87 cell line, we identified significant changes in gene expression among resistant and drug-naïve cells. We focused on the striking difference (>10 fold) in the gene expression of QPRT that was upregulated in cells resistant to panobinostat, bortezomib, and their combination and validated this difference in expression at the protein level for the pediatric glioma cell lines, SJG 2 and DIPG 007. Reducing QPRT expression with RNA interference re-sensitized the resistant U87 and SJG 2 cells to the panobinostat-bortezomib combination indicating that QPRT has a major role in engendering resistance. Consistent with QPRT's known function of catalyzing the rate limiting step in de novo NAD+ biosynthesis from tryptophan, the NAD + levels in all three resistant cell lines were elevated 4–7-fold in comparison to their drug naïve counterparts suggesting that elevated NAD+ biosynthesis is a dependency of panobinostat-bortezomib resistance. Although selective inhibitors of QPRT enzymatic activity are not available to pharmacologically test this hypothesis directly, we treated the resistant cells with FK866, a selective inhibitor of the NAD+ salvage pathway reasoning that these cells would also be dependent on this pathway to maintain the elevated levels of NAD + necessary to preserve viability of the resistant cells. FK866 treatment lowered NAD+ levels and specifically induced apoptosis in the resistant cells compared to the drug naïve cells in the absence of panobinostat and bortezomib highlighting the exquisite dependence of panobinostat-bortezomib resistant cell viability on elevated NAD+ levels. Based on this observation, we tested the corollary that panobinostat-bortezomib resistant cell viability depended on NAD+-consuming reactions such as those catalyzed by PARP and sirtuins. Like FK866, the PARP1 inhibitor, niraparib, and the sirtuin1 inhibitor, selisistat each induced apoptosis specifically in the resistant versus drug naïve cells thereby supporting this hypothesis. Strikingly, the combination of FK866 and niraparib induced >90% apoptosis in the panobinostat-bortezomib resistant cells without a discernable effect on the drug naïve cells. Together, these results demonstrate the non-oncogene addiction of panobinostat-bortezomib resistant cells to elevated NAD+ and correspondingly, to the cellular processes that consume this coenzyme. Teleologically, the elevated expression of QPRT offers a solution to satisfying NAD+ addiction in tumors such as high-grade gliomas (i.e., GBM) where amplification of either the NAD+ salvage pathway or the alternative pathway for de novo synthesis from nicotinic acid (i.e., Preiss-Handler pathway) would not be expected (42).

The extensive and non-overlapping changes in gene expression across all three cell lines that accompany treatment with the pleiotropic agents, panobinostat and bortezomib would

Author Manuscript Author Manuscript Author Manuscript Author Manuscript

suggest the need for widespread compensatory dysregulation to confer resistance. The selection of an altered NAD+ metabolic state has the potential to meet this need. NAD+ is a cofactor for multiple oxidoreductases (43) and a substrate for PARPs thereby having the ability to control drug-induced oxidative and replicative stress, respectively (44, 45). The increased sensitivity of the resistant cells to a PARP inhibitor and the identification of 5-fluorouracil and gemcitabine as de novo vulnerabilities of the resistant state support the latter. Likewise, this study suggests the important role of NAD+ regulated sirtuins and their ability to extensively alter the epigenetic landscape through their deacetylation of histones and transcription factors (46, 47). Interestingly, RNA-seq analysis identified nicotinamide N-methyltransferase (NNMT) as being upregulated in the drug resistant DIPG-007 cell line in comparison to the corresponding drug naïve cells. NNMT methylates nicotinamide (NAM), the product of PARP and sirtuin NAD+ consumption (Fig. 4D), uses S-adenosylmethionine (SAM) and has been shown to regulate SAM levels and correspondingly other SAM-dependent methyl transferases to significantly alter the epigenetic landscape in cancer cells (48, 49). N-methyl-NAM has also been shown to selectively increase protein expression of Sirt 1 by blocking Sirt 1 ubiquination and subsequent proteasome-mediated degradation without a general effect on the latter (50). By analogy, it is tempting to speculate that the enhanced protein expression of QPRT that appears in part to be post translationally regulated may involve N-methyl-NAM. These observations together with the results of our study, suggest that the highly integrated NAD+ metabolic network has the potential to engender resistance to combinations of pleiotropic agents and this convergent mechanism of resistance offers defined therapeutic opportunities. Future complementary studies involving the implementation of a comprehensive in situ hyperplexed proteomic analysis of patient glioma samples having subcellular resolution (51) may enable additional insights into the dysregulation of the NAD+ metabolic network. The knowledge gained from these analyses could guide the development of preclinical models that recapitulate intracellular and intercellular signaling interactions to help define the role of the tumor microenvironment (see below) and accordingly, indicate emergent drug targets.

This study was performed under cell autonomous conditions indicating a potential limitation as the tumor microenvironment could impact drug sensitivity and/or the selection of drug resistant mechanisms. For example although under these conditions we demonstrated a QPRT dependency for resistance to bortezomib and panobinostat, it has been suggested that the association of high QPRT expression with radio-chemotherapy resistance observed in the clinic (27) may in part be dependent on the microglia supplying quinolinic acid, the substrate for QPRT. After submission of our work, an independent study exploiting large scale drug combination screening demonstrated the sensitivity of other diffuse midline glioma cell lines to the combination of panobinostat and marizomib, like bortezomib another proteasome inhibitor (31). Although the screening was also performed under cell autonomous conditions, a significant increase in survival, albeit modest, was demonstrated with this combination in orthotopic xenograft models. Interestingly, although the precise mechanism of tumor cytotoxicity was not defined, depletion of NAD+ was implicated (31). Our study, by demonstrating that the selection of resistance to a similar drug combination involved enhanced NAD+ biosynthesis is complementary to Lin et al (31) and importantly informs a therapeutic strategy involving NAD+ biosynthesis inhibition to further improve

Author Manuscript Author Manuscript Author Manuscript Author Manuscript

glioma patient survival. Future studies, perhaps those involving cerebral organoid models (52) will be required to determine the impact of the tumor microenvironment on the evolution of resistance to combinations of panobinostat with proteasome inhibitors. Finally, QPRT has been reported to interact with caspase 3 and reduce its apoptotic activity (53). Therefore, complementary to our study it would be important to determine the contribution of possible NAD+ metabolic network independent effects of QPRT (53, 54) for conferring resistance in glioma.

Supplementary Material

Refer to Web version on PubMed Central for supplementary material.

Acknowledgements

This work was supported by the Connor's Cure Foundation Fund, the Translational Brain Tumor Research Fund, and the Scientific Program Fund of the Children's Hospital of Pittsburgh Foundation (all to Ian F. Pollack). D. Lansing Taylor, Mark Schurdak and Andrew Stern were supported by the University of Pittsburgh Cancer Institute (UPCI) Chemical Biology Facility that is funded in part by award P30CA047904, the NIH-National Cancer Institute, Cancer Center Support Grant, to the UPCI. The authors thank Alexis Styche for FACS analysis.

List of abbreviations:

BSA	bovine serum albumin
DMSO	dimethyl sulfoxide
DSB	double strand break
EGF	epidermal growth factor
FACS	fluorescence activated cell sorting
FGF	fibroblast growth factor
FITC	fluorescein isothiocyanate
NAD	nicotinamide adenine dinucleotide
NAM	nicotinamide
NNMT	nicotinamide N-methyltransferase
PARP	poly (ADP-ribose) polymerase
PBS	phosphate-buffered saline
PAGE	polyacrylamide gel electrophoresis
SAM	S-adenosylmethionine
SIRT	silent information regulator
TBS	Tris-buffered saline
PARP	poly ADP-ribose polymerase

Author Manuscript Author Manuscript Author Manuscript Author Manuscript

PDGF	Platelet-derived growth factor
PI	propidium iodide
TBS	Tris-buffered saline
QPRT	Quinolate phosphoribosyltransferase

References

1. Buckner J, Giannini C, Eckel-Passow J, Lachance D, Parney I, Laack N, et al. Management of diffuse low-grade gliomas in adults - use of molecular diagnostics. Nat Rev Neurol 2017;136:340–51.
2. Reifenberger G, Wirsching HG, Knobbe-Thomsen CB, Weller M. Advances in the molecular genetics of gliomas - implications for classification and therapy. Nat Rev Clin Oncol 2017;147:434–52.
3. Wen PY, Reardon DA. Neuro-oncology in 2015: Progress in glioma diagnosis, classification and treatment. Nat Rev Neurol 2016;122:69–70.
4. Tanaka S, Louis DN, Curry WT, Batchelor TT, Dietrich J. Diagnostic and therapeutic avenues for glioblastoma: no longer a dead end? Nat Rev Clin Oncol 2013;101:14–26.
5. Grasso CS, Tang Y, Truffaux N, Berlow NE, Liu L, Debily MA, et al. Functionally defined therapeutic targets in diffuse intrinsic pontine glioma. Nat Med 2015;216:555–9.
6. Reardon DA, Wen PY. Glioma in 2014: unravelling tumour heterogeneity-implications for therapy. Nat Rev Clin Oncol 2015;122:69–70.
7. McCracken DJ, Celano EC, Voloschin AD, Read WL, Olson JJ. Phase I trial of dose-escalating metronomic temozolomide plus bevacizumab and bortezomib for patients with recurrent glioblastoma. J Neurooncol 2016;1301:193–201.
8. Premkumar DR, Jane EP, Agostino NR, DiDomenico JD, Pollack IF. Bortezomib-induced sensitization of malignant human glioma cells to vorinostat-induced apoptosis depends on reactive oxygen species production, mitochondrial dysfunction, Noxa upregulation, Mcl-1 cleavage, and DNA damage. Mol Carcinog 2013;522:118–33.
9. Bhatia R, Calvo KC. The sequencing expression, purification, and steady-state kinetic analysis of quinolinate phosphoribosyl transferase from Escherichia coli. Arch Biochem Biophys 1996;3252:270–8.
10. Cao H, Pietrak BL, Grubmeyer C. Quinolinate phosphoribosyltransferase: kinetic mechanism for a type II PRTase. Biochemistry 2002;4110:3520–8.
11. Premkumar DR, Jane EP, Thambireddy S, Sutera PA, Cavaleri JM, Pollack IF. Mitochondrial dysfunction RAD51, and Ku80 proteolysis promote apoptotic effects of Dinaciclib in Bcl-xL silenced cells. Mol Carcinog 2018;574:469–82.
12. Meel MH, Sewing ACP, Waranecki P, Metselaar DS, Wedekind LE, Koster J, et al. Culture methods of diffuse intrinsic pontine glioma cells determine response to targeted therapies. Exp Cell Res 2017;3602:397–403.
13. Jane EP, Premkumar DR, Cavaleri JM, Sutera PA, Rajasekar T, Pollack IF. Dinaciclib, a Cyclin-Dependent Kinase Inhibitor Promotes Proteasomal Degradation of Mcl-1 and Enhances ABT-737-Mediated Cell Death in Malignant Human Glioma Cell Lines. J Pharmacol Exp Ther 2016;3562:354–65.
14. Meel MH, Metselaar DS, Waranecki P, Kaspers GJL, Hulleman E. An efficient method for the transduction of primary pediatric glioma neurospheres. MethodsX 2018;5:173–83. [PubMed: 30622915]
15. Rai M, Soragni E, Chou CJ, Barnes G, Jones S, Rusche JR, et al. Two new pimelic diphenylamide HDAC inhibitors induce sustained frataxin upregulation in cells from Friedreich's ataxia patients and in a mouse model. PLoS One 2010;51:e8825.
16. West AC, Johnstone RW. New and emerging HDAC inhibitors for cancer treatment. J Clin Invest 2014;1241:30–9.

Author Manuscript Author Manuscript Author Manuscript Author Manuscript

17. Asklund T, Kvarnbrink S, Holmlund C, Wibom C, Bergenheim T, Henriksson R, et al. Synergistic killing of glioblastoma stem-like cells by bortezomib and HDAC inhibitors. Anticancer Res 2012;327:2407–13.
18. Friday BB, Anderson SK, Buckner J, Yu C, Giannini C, Geoffroy F, et al. Phase II trial of vorinostat in combination with bortezomib in recurrent glioblastoma: a north central cancer treatment group study. Neuro Oncol 2012;142:215–21.
19. Yu C, Friday BB, Yang L, Atadja P, Wigle D, Sarkaria J, et al. Mitochondrial Bax translocation partially mediates synergistic cytotoxicity between histone deacetylase inhibitors and proteasome inhibitors in glioma cells. Neuro Oncol 2008;103:309–19.
20. Youn HS, Kim TG, Kim MK, Kang GB, Kang JY, Lee JG, et al. Structural Insights into the Quaternary Catalytic Mechanism of Hexameric Human Quinolinate Phosphoribosyltransferase, a Key Enzyme in de novo NAD Biosynthesis. Sci Rep 2016;6:19681. [PubMed: 26805589]
21. Harris LW, Lockstone HE, Khaitovich P, Weickert CS, Webster MJ, Bahn S. Gene expression in the prefrontal cortex during adolescence: implications for the onset of schizophrenia. BMC Med Genomics 2009;2:28. [PubMed: 19457239]
22. Murat A, Migliavacca E, Gorlia T, Lambiv WL, Shay T, Hamou MF, et al. Stem cell-related “self-renewal” signature and high epidermal growth factor receptor expression associated with resistance to concomitant chemoradiotherapy in glioblastoma. J Clin Oncol 2008;2618:3015–24.
23. Paugh BS, Broniscer A, Qu C, Miller CP, Zhang J, Tatevossian RG, et al. Genome-wide analyses identify recurrent amplifications of receptor tyrosine kinases and cell-cycle regulatory genes in diffuse intrinsic pontine glioma. J Clin Oncol 2011;2930:3999–4006.
24. Paugh BS, Qu C, Jones C, Liu Z, Adamowicz-Brice M, Zhang J, et al. Integrated molecular genetic profiling of pediatric high-grade gliomas reveals key differences with the adult disease. J Clin Oncol 2010;2818:3061–8.
25. Reifenberger G, Weber RG, Riehmer V, Kaulich K, Willscher E, Wirth H, et al. Molecular characterization of long-term survivors of glioblastoma using genome- and transcriptome-wide profiling. Int J Cancer 2014;1358:1822–31.
26. Sturm D, Witt H, Hovestadt V, Khuong-Quang DA, Jones DT, Konermann C, et al. Hotspot mutations in H3F3A and IDH1 define distinct epigenetic and biological subgroups of glioblastoma. Cancer Cell 2012;224:425–37.
27. Sahm F, Oezen I, Opitz CA, Radlwimmer B, von Deimling A, Ahrendt T, et al. The endogenous tryptophan metabolite and NAD+ precursor quinolinic acid confers resistance of gliomas to oxidative stress. Cancer Res 2013;7311:3225–34.
28. Chiarugi A, Dolle C, Felici R, Ziegler M. The NAD metabolome--a key determinant of cancer cell biology. Nat Rev Cancer 2012;1211:741–52.
29. Pei F, Li H, Henderson MJ, Titus SA, Jadhav A, Simeonov A, et al. Connecting Neuronal Cell Protective Pathways and Drug Combinations in a Huntington’s Disease Model through the Application of Quantitative Systems Pharmacology. Sci Rep 2017;71:17803.
30. Jagannath S, Dimopoulos MA, Lonial S. Combined proteasome and histone deacetylase inhibition: A promising synergy for patients with relapsed/refractory multiple myeloma. Leuk Res 2010;349:1111–8.
31. Lin GL, Wilson KM, Ceribelli M, Stanton BZ, Woo PJ, Kreimer S, et al. Therapeutic strategies for diffuse midline glioma from high-throughput combination drug screening. Sci Transl Med 2019;11519.
32. Di K, Lloyd GK, Abraham V, MacLaren A, Burrows FJ, Desjardins A, et al. Marizomib activity as a single agent in malignant gliomas: ability to cross the blood-brain barrier. Neuro Oncol 2016;186:840–8.
33. Gozzetti A, Papini G, Candi V, Brambilla CZ, Sirianni S, Bocchia M. Second Generation Proteasome Inhibitors in Multiple Myeloma. Anticancer Agents Med Chem 2017;177:920–26.
34. Manton CA, Johnson B, Singh M, Bailey CP, Bouchier-Hayes L, Chandra J. Induction of cell death by the novel proteasome inhibitor marizomib in glioblastoma in vitro and in vivo. Sci Rep 2016;6:18953. [PubMed: 26804704]
35. Rabal O, Sanchez-Arias JA, Cuadrado-Tejedor M, de Miguel I, Perez-Gonzalez M, Garcia-Barroso C, et al. Design, Synthesis, and Biological Evaluation of First-in-Class Dual Acting Histone

Author Manuscript Author Manuscript Author Manuscript Author Manuscript

Deacetylases (HDACs) and Phosphodiesterase 5 (PDE5) Inhibitors for the Treatment of Alzheimer's Disease. J Med Chem 2016;5919:8967–9004.

36. Mandel JJ, Youssef M, Ludmir E, Yust-Katz S, Patel AJ, De Groot JF. Highlighting the need for reliable clinical trials in glioblastoma. Expert Rev Anticancer Ther 2018;1810:1031–40.
37. Lee P, Murphy B, Miller R, Menon V, Banik NL, Giglio P, et al. Mechanisms and clinical significance of histone deacetylase inhibitors: epigenetic glioblastoma therapy. Anticancer Res 2015;352:615–25.
38. Thomas AA, Brennan CW, DeAngelis LM, Omuro AM. Emerging therapies for glioblastoma. JAMA Neurol 2014;7111:1437–44.
39. Thibaudeau TA, Smith DM. A Practical Review of Proteasome Pharmacology. Pharmacol Rev 2019;712:170–97.
40. Easwaran H, Tsai HC, Baylin SB. Cancer epigenetics: tumor heterogeneity, plasticity of stem-like states, and drug resistance. Mol Cell 2014;545:716–27.
41. Sharma SV, Lee DY, Li B, Quinlan MP, Takahashi F, Maheswaran S, et al. A chromatin-mediated reversible drug-tolerant state in cancer cell subpopulations. Cell 2010;1411:69–80.
42. Chowdhry S, Zanca C, Rajkumar U, Koga T, Diao Y, Raviram R, et al. NAD metabolic dependency in cancer is shaped by gene amplification and enhancer remodelling. Nature 2019;5697757:570–75.
43. Verdin E NAD(+) in aging, metabolism, and neurodegeneration. Science 2015;3506265:1208–13.
44. Vyas S, Chang P. New PARP targets for cancer therapy. Nat Rev Cancer 2014;147:502–9.
45. Gupte R, Liu Z, Kraus WL. PARPs and ADP-ribosylation: recent advances linking molecular functions to biological outcomes. Genes Dev 2017;312:101–26.
46. Chalkiadaki A, Guarente L. The multifaceted functions of sirtuins in cancer. Nat Rev Cancer 2015;1510:608–24.
47. Houtkooper RH, Canto C, Wanders RJ, Auwerx J. The secret life of NAD+: an old metabolite controlling new metabolic signaling pathways. Endocr Rev 2010;312:194–223.
48. Ulanovskaya OA, Zuhl AM, Cravatt BF. NNMT promotes epigenetic remodeling in cancer by creating a metabolic methylation sink. Nat Chem Biol 2013;95:300–6.
49. Pissios P Nicotinamide N-Methyltransferase: More Than a Vitamin B3 Clearance Enzyme. Trends Endocrinol Metab 2017;285:340–53.
50. Hong S, Moreno-Navarrete JM, Wei X, Kikukawa Y, Tzameli I, Prasad D, et al. Nicotinamide N-methyltransferase regulates hepatic nutrient metabolism through Sirt1 protein stabilization. Nat Med 2015;218:887–94.
51. Spagnolo DM, Al-Kofahi Y, Zhu P, Lezon TR, Gough A, Stern AM, et al. Platform for Quantitative Evaluation of Spatial Intratumoral Heterogeneity in Multiplexed Fluorescence Images. Cancer Res 2017;7721:e71–e74.
52. Linkous A, Balamatsias D, Snuderl M, Edwards L, Miyaguchi K, Milner T, et al. Modeling Patient-Derived Glioblastoma with Cerebral Organoids. Cell Rep 2019;2612:3203–11 e5.
53. Ishidoh K, Kamemura N, Imagawa T, Oda M, Sakurai J, Katunuma N. Quinolinate phosphoribosyl transferase, a key enzyme in de novo NAD(+) synthesis, suppresses spontaneous cell death by inhibiting overproduction of active-caspase-3. Biochim Biophys Acta 2010;18035:527–33.
54. Ullmark T, Montano G, Jarvstrat L, Jernmark Nilsson H, Hakansson E, Drott K, et al. Anti-apoptotic quinolinate phosphoribosyltransferase (QPRT) is a target gene of Wilms' tumor gene 1 (WT1) protein in leukemic cells. Biochem Biophys Res Commun 2017;4824:802–07.

Author Manuscript Author Manuscript Author Manuscript Author Manuscript

Implications:

These data provide new insights into mechanisms of treatment resistance in gliomas, hold promise for targeting recurrent disease, and provide a potential strategy for further exploration of next generation inhibitors.

Author Manuscript Author Manuscript Author Manuscript Author Manuscript

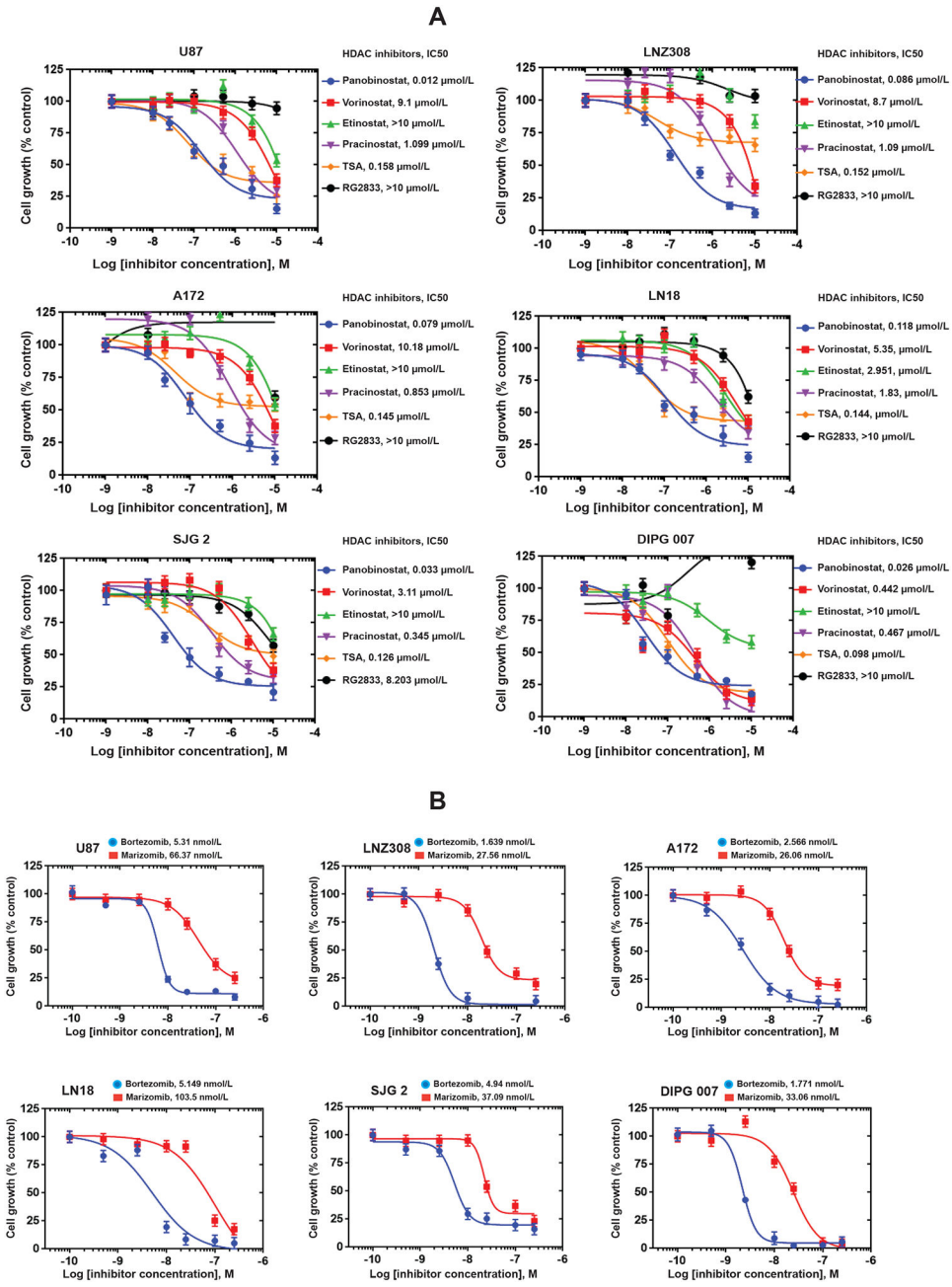

Figure 1. Effect of HDAC and proteasome inhibitors on cell proliferation inhibition in malignant human glioma cell lines.

Dose response curves of a panel of glioma cell lines (U87, LNZ308, A172, LN18, SJG 2 and DIPG 007) treated with indicated histone deacetylase inhibitors (**A**, Panobinostat, vorinostat, entinostat, pracinostat, trichostatin A, and RG2833) or proteasome inhibitors (**B**, bortezomib or marizomib). Cells (3×10^3) were seeded on 96-well plates, and, the following day, were exposed to indicated concentrations of inhibitors (equal volume of 2x concentrations). Control cells received vehicle (DMSO, 0) for 72 h. Cell proliferation inhibition was assessed semiquantitatively by spectrophotometric measurement of MTS bioreduction as described in the Materials and Methods. $n = 4$ wells per condition. All

Author Manuscript Author Manuscript Author Manuscript Author Manuscript

experiments were performed at least three times. The inhibitor concentrations required to reduce cell growth by 50% (IC50) were calculated by plotting the percent inhibition in proliferation in inhibitor-treated cells compared to vehicle-treated cells using GraphPad Prism version 6.0 software (GraphPad Software).

Author Manuscript Author Manuscript Author Manuscript Author Manuscript

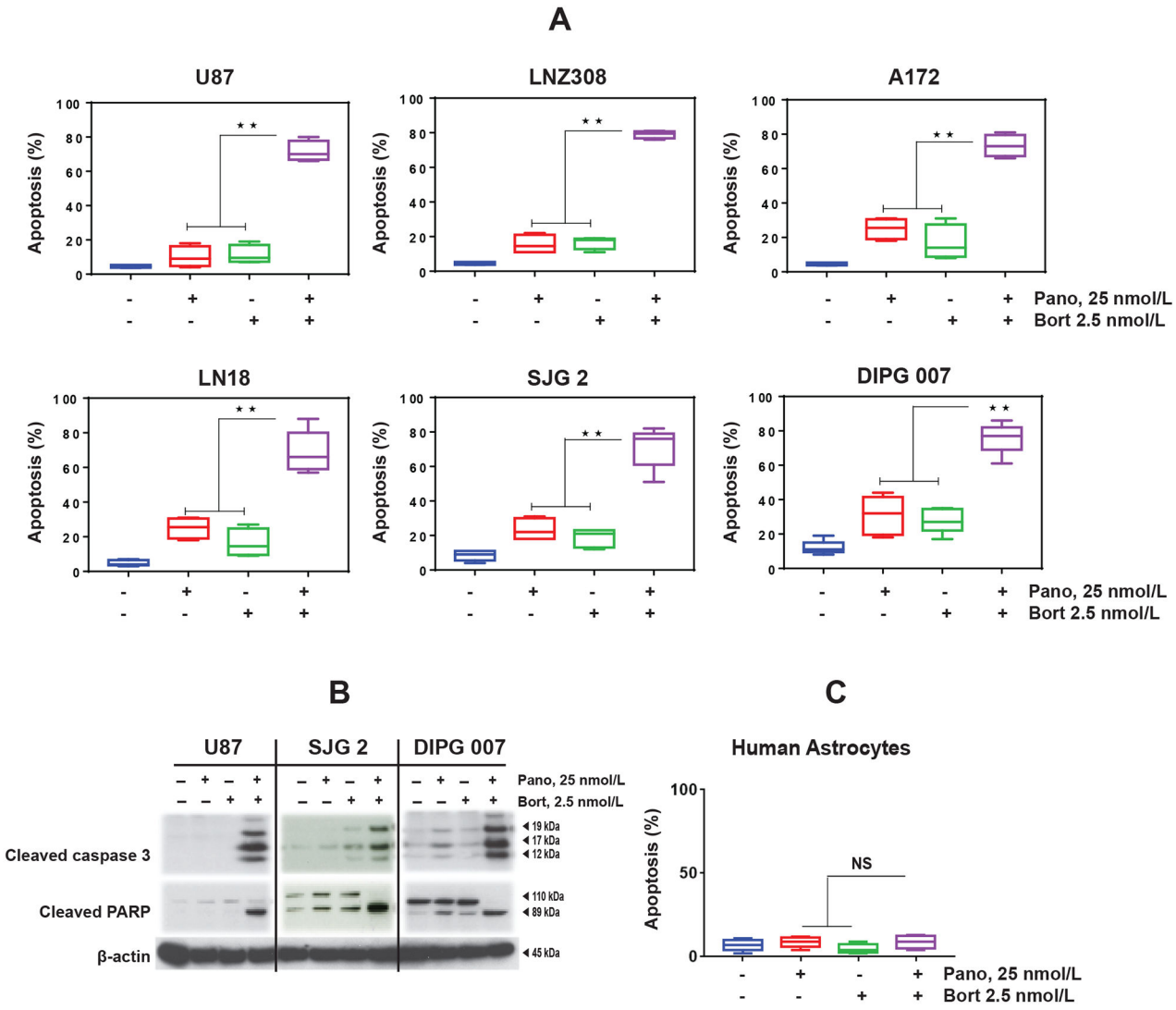

Figure 2. Cotreatment with bortezomib enhances the efficacy of panobinostat.

A. U87, LNZ308, A172, LN18, SJG 2 and DIPG 007 cells were seeded in 6-well plates and treated with panobinostat (25 nmol/L, Pano), bortezomib (2.5 nmol/L, Bort) or both in combination. Apoptosis was analyzed by Annexin assay using flow cytometry. The results represent the mean of 3 three independent experiments (**, $p < 0.005$; single agent versus combination of both). **B.** U87, SJG 2 and DIPG 007 cells were treated with panobinostat (Pano, 25 nmol/L) or bortezomib (Bort, 2.5 nmol/L) or the combination of both (panobinostat, 25 nmol/L plus bortezomib, 2.5 nmol/L) for 72 h. Control cells received DMSO. Whole cell extracts were prepared, and equal amounts of protein were separated by SDS-PAGE and subjected to Western blot analysis with the indicated antibodies. B-actin served as loading control. The images from a representative study are shown. Two additional experiments produced similar results. **C**. Non-neoplastic human astrocytes were exposed to inhibitors as described in **A**. Control cells received vehicle (DMSO) for 72 h. Apoptosis was analyzed by flow cytometry. The results represent the mean of three independent experiments (single agent versus combination of both; NS, not significant).

Author Manuscript Author Manuscript Author Manuscript Author Manuscript

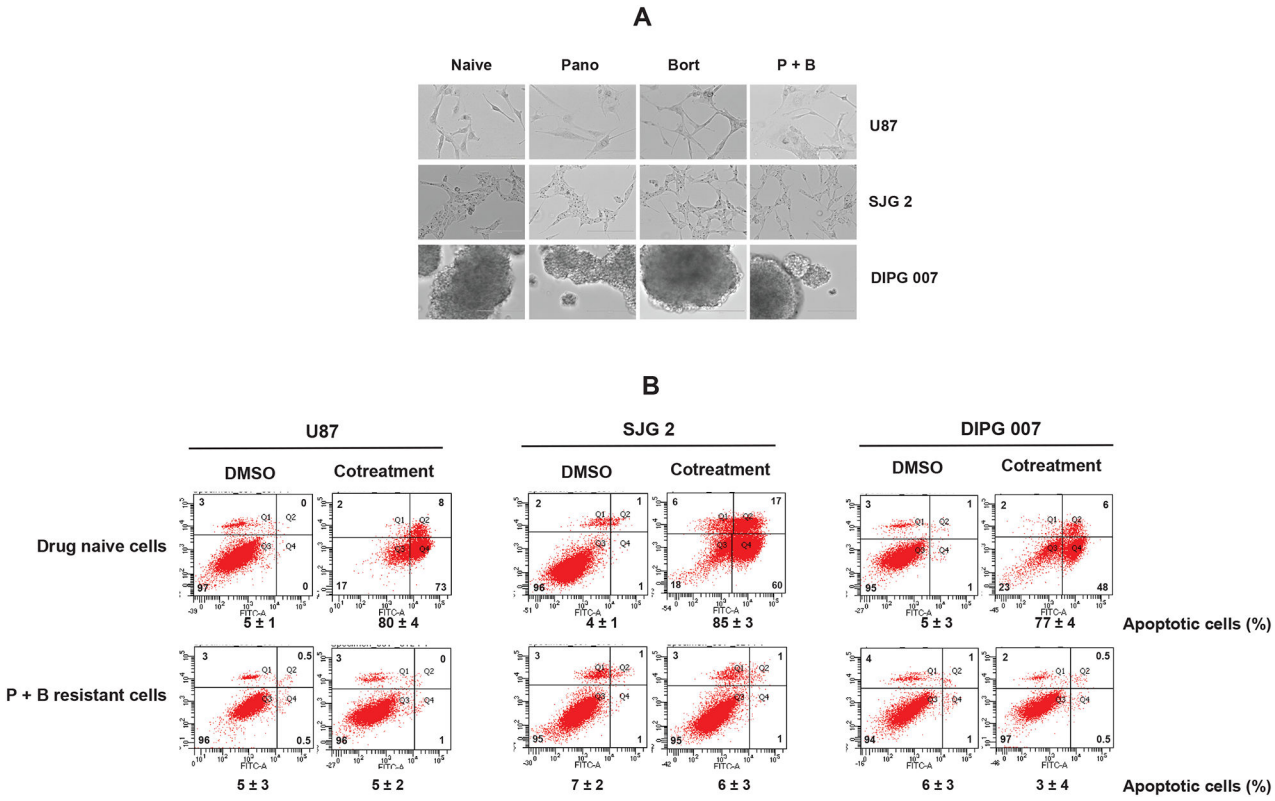

Figure 3. Acquired resistance to panobinostat and bortezomib.

A. Drug naïve or panobinostat-resistant (Pano), bortezomib-resistant (Bort), or panobinostat and bortezomib resistant (P + B) cells were seeded and morphology was evaluated by microscopic inspection (scale bar, 200 micron). **B.** Drug naïve (upper panel) and panobinostat and bortezomib resistant (P + B resistant, lower panel) cells were seeded and cotreated with panobinostat (25 nmol/L) plus bortezomib (2.5 nmol/L) for 72 h. Control cells received an equivalent amount of vehicle (DMSO). Apoptosis was assessed by Annexin V-FITC and propidium iodide (PI) staining and FACS analysis as described in the Materials and Methods. The representative FACS histogram with the percentages of cells in each quadrant are indicated. Annexin V is plotted on the x-axis, and PI is plotted on the y-axis. Cells in the lower left quadrant reflect live cells; cells in the lower right quadrant (annexin V positive) represent early apoptotic cells; cells in the upper right quadrant (annexin V/PI positive) represent late apoptotic cells; cells in the upper left quadrant (PI positive) represent dead cells. The results (annexin V and/or PI positive cells) from the mean of three independent experiments for each cell type are given below.

Author Manuscript Author Manuscript Author Manuscript Author Manuscript

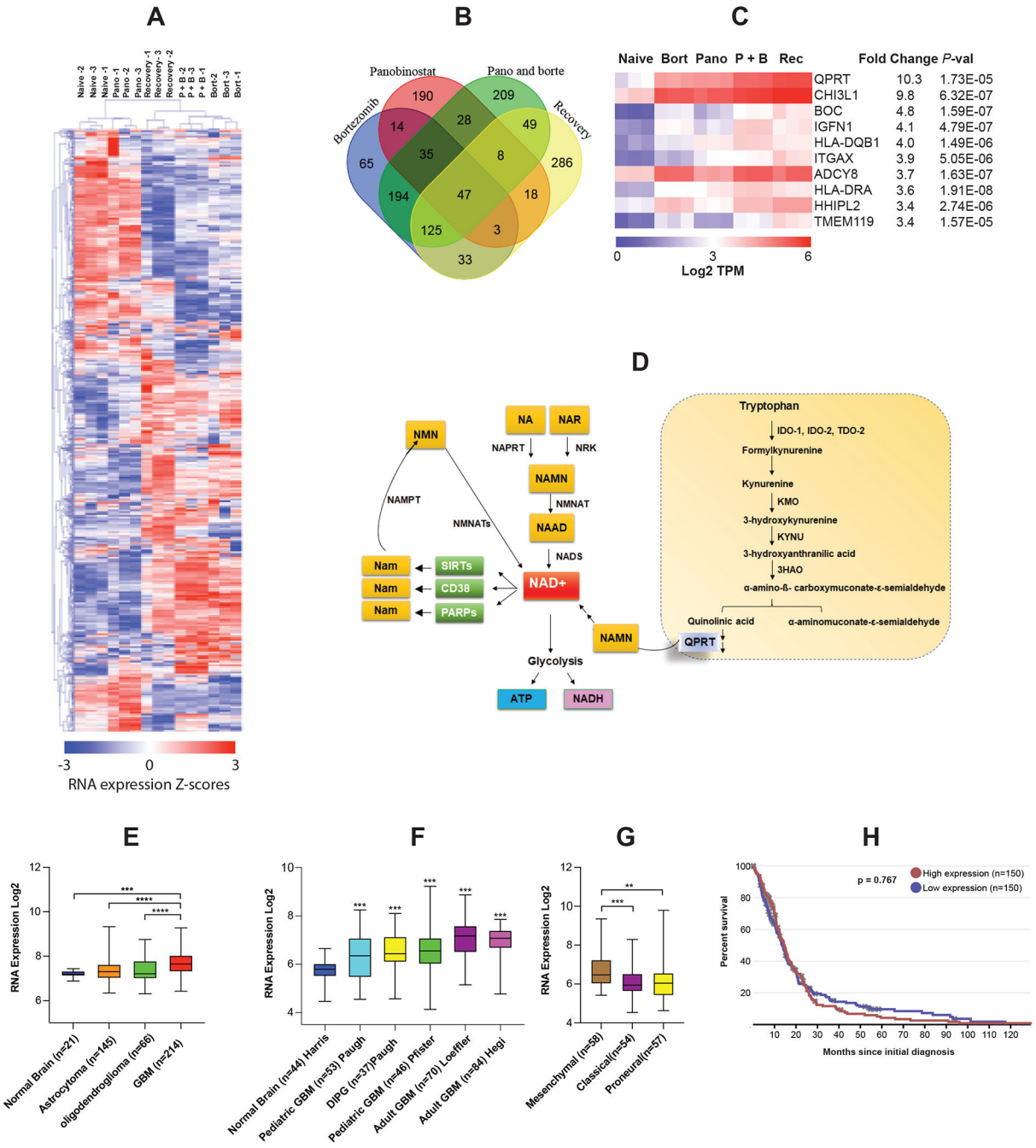

Figure 4. Sustained inhibition of HDAC and proteasome activity leads to unique changes in gene expression.

A. Hierarchical clustering comparing drug naïve (Naive), panobinostat-resistant (Pano), bortezomib-resistant (Bort), panobinostat and bortezomib-resistant (P + B) or recovered U87 cells (Recovery, i.e. inhibitors removed for 30 days). In the heatmap presentation, each row represents a gene and each column represents a sample (3 biological replicates). **B**. Venn Diagram indicating number of genes overlapped between comparisons. **C**. Heatmap representing the log2 of normalized transcript counts per million (TPM) of the top 10 genes differentially expressed in bortezomib-resistant (Bort), panobinostat-resistant (Pano),

Author Manuscript Author Manuscript Author Manuscript Author Manuscript

panobinostat and bortezomib-resistant (P + B) and recovery cells (Rec) compared to control U87 non-treated cells (naïve). **D.** Model depicting intracellular NAD+ synthesis and NAD+-consuming pathways. The kynurenine de novo biosynthesis (boxed in dotted line) begins with the conversion of tryptophan to formylkynurenine either by indoleamine dioxygenase (IDO) or tryptophan dioxygenase (TDO). The kynurenine is used as substrate by kynurenine monooxygenase (KMO) to form 3-hydroxykynurenine. The kynureninase (KYNU) forms 3-hydroxyanthranilate, which is subsequently converted to α-amino-ß-carboxymuconate-ε-semialdehyde by 3-hydroxyanthranilate dioxygenase (3HAO). Then α-amino-ß-carboxymuconate-ε-semialdehyde subsequently converted to quinolinic acid. Then, quinolinic acid is converted to NAMN by quinolate phosphoribosyltransferase (QPRT) used for NAD+ biosynthesis. NAD+ is also synthesized from vitamin B3 (niacin), either in nicotinic acid (NA) or nicotinamide (Nam), which is converted to respective mononucleotides (NAMN and NMN) by NA phosphoribosyltransferase (NAPRT, via Preiss-Handler pathway) or Nam phosphoribosyltransferase (NAMPT, via salvage pathway). NAD + generated from kynurenine de novo /salvage pathways are consumed by sirtuins, poly (ADP-ribose) polymerases (PARPs) and CD38 and leads to the generation of Nam. Additionally, another pathway utilizing NAD+ is reduction to nicotinamide adenine dinucleotide (NADH) during metabolic processes such as glycolysis, leading to the generation of ATP. **E**. QPRT mRNA expression across several glioma tumors compared with normal brain in the REMBRANDT dataset. **F.** Metanalysis performed in R2 genomics software comparing normal brain (cortex) to 136 pediatric Gliomas (high grade gliomas, Paugh n=53 and Pfister n=46 and DIPG, Paugh n=37) and 154 Adult GBM (loeffler n=70 and Hegi n=84), QPRT mRNA was significantly upregulated compared to normal brain across all data sets (21–26); *** P< 0.001. **G.** QPRT mRNA expression amongst glioblastoma subtypes (TCGA n = 172). **H**. QPRT high gene expression based on median RNA cutoff value is not associated with overall survival, p-value 0.767 (log rank test), TCGA.

Author Manuscript Author Manuscript Author Manuscript Author Manuscript

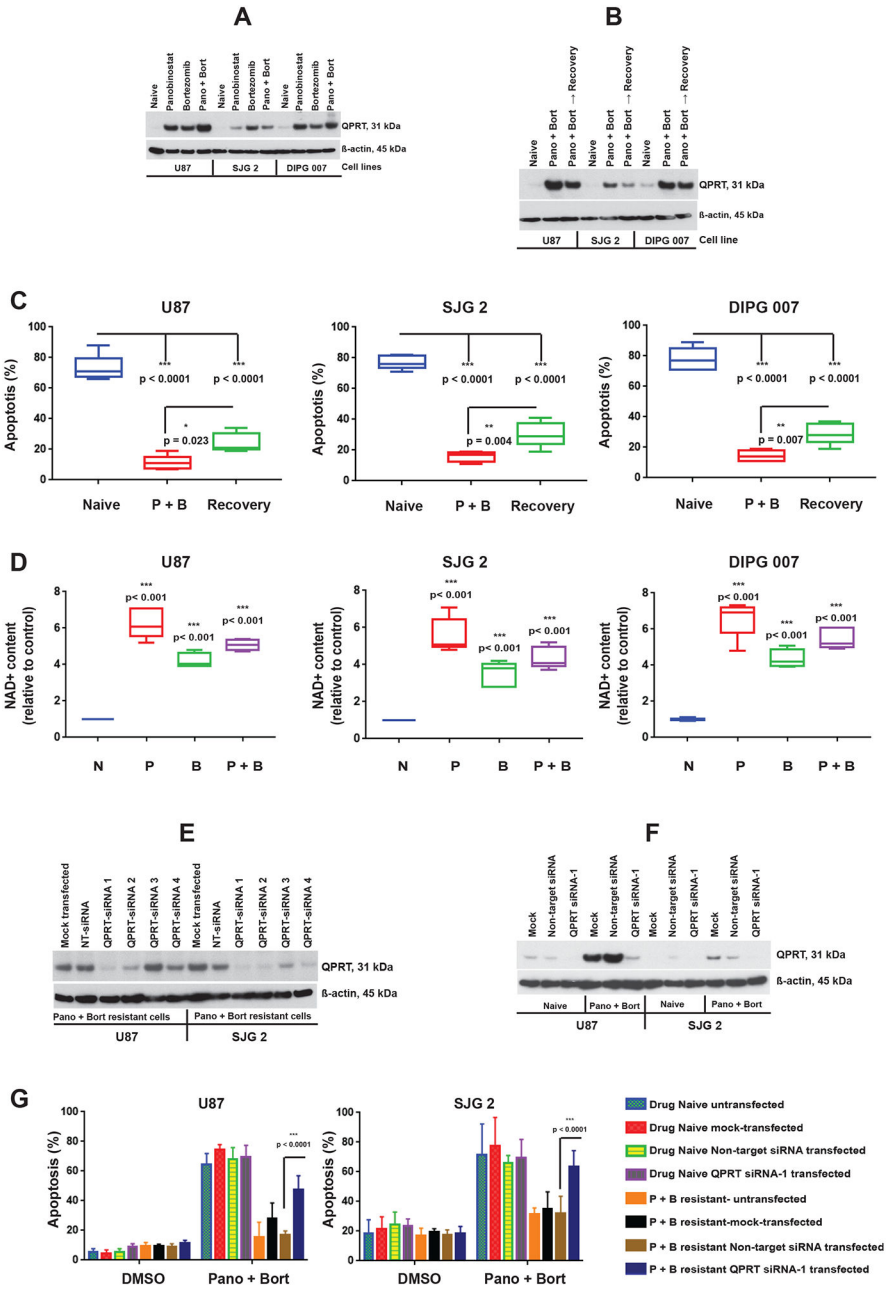

Figure 5. Sustained inhibition of HDAC and proteasome activity upregulate QPRT expression in glioma cells.

A and **B** Whole cell lysates from naïve, panobinostat-resistant (panobinostat), bortezomib-resistant (bortezomib) or panobinostat and bortezomib-resistant cells (Pano+ Bort), or recovery cells (Pano+ Bort → Recovery, inhibitors removed for 30 days) were subjected to Western blot analysis. Equal amounts of protein were separated by SDS-PAGE and subjected to Western blot analysis with the indicated antibodies. β-actin served as loading control. The images from a representative study are shown. Two additional experiments produced similar results. **C.** Drug naïve or panobinostat and bortezomib-resistant (P + B) and recovery cells were allowed to attach overnight and cotreated with panobinostat (25

Author Manuscript Author Manuscript Author Manuscript Author Manuscript

nmol/L) and bortezomib (2.5 nmol/L) for 72 h. Cell viability was assessed by annexin V and propidium iodide assay. The results represent the mean of 3 three independent experiments. Error bars indicate ± SD. Results were analyzed for statistical significance by ANOVA (Tukey's HSD multiple comparison). **D**. Cellular NAD+ levels in drug naïve (N) or panobinostat-resistant (P), bortezomib-resistant (B), panobinostat plus bortezomib-resistant (P + B). The NAD+ level was measured by commercially available kit according to the manufacturer's recommendation as described in the Materials and Methods and reported as fold change relative to control. All data are representative of three independent experiments (naïve versus resistant cells; unpaired two-tailed *t* test). **E.** Panobinostat and bortezomib resistant U87 or SJG 2 cells were either mock transfected (no siRNA) or non-target siRNA (NT siRNA) or four QPRT siRNAs (QPRT siRNA 1 – 4) as described in the Materials and Methods. Equal amounts of protein were separated by SDS-PAGE and subjected to Western blot analysis with the indicated antibodies. β-actin served as loading control. The images from a representative study are shown. **F**. Drug naïve or panobinostat and bortezomib resistant (Pano + Bort) cells (U87 and SJG 2) were transfected as described in the Materials and Methods and protein was subjected to Western blot analysis using indicated antibodies. β-actin served as loading control. **G.** 72 h post-transfection, cells were treated with DMSO or panobinostat, 25 nmol/L plus bortezomib, 2.5 nmol/L (Pano + Bort). Cell viability assay was performed after 3 days. Error bars indicate ± SD. Results were analyzed by Tukey's ANOVA.

Author Manuscript Author Manuscript Author Manuscript Author Manuscript

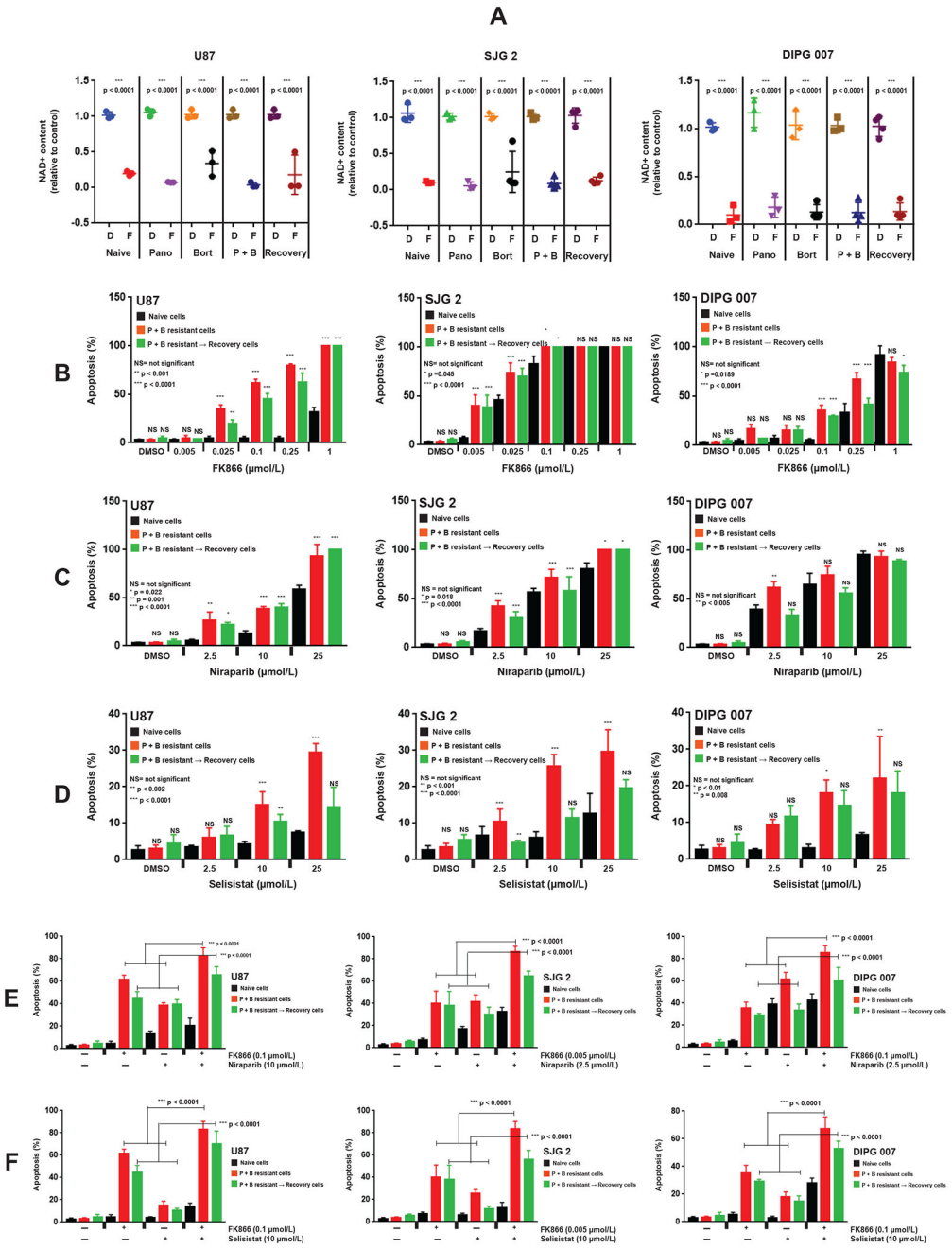

Figure 6. Targeting NAD+ biosynthesis pathway overcomes panobinostat and bortezomib-induced resistance.

A. Drug naïve, panobinostat resistant (Pano), bortezomib resistant (Bort) or dual inhibitor resistant (P + B) or recovery cells were exposed to DMSO (D) or FK866 (F). U87 and DIPG 007 cells were treated with 0.1 μmol/L, whereas SJG 2 cells with 0.005 μmol/L FK866 for 72 h. The NAD+ levels were measured as described in the Materials and Methods. Values reported as fold change normalized to control. All data are representative of three independent experiments. Error bars indicate ± SD (control versus FK866-treated; unpaired two-tailed t test). **B-D.** Drug naive or panobinostat and bortezomib-resistant (P + B resistant

Author Manuscript Author Manuscript Author Manuscript Author Manuscript

cells) or recovery cells (inhibitor removed for 30 days, P + B→ recovery) cells were seeded on 6-well plates (U87, left panel; SJG 2 middle panel; DIPG 007, right panel). The following day, cells were exposed to indicated concentration of FK866 (**B**) or niraparib (**C**) or selisistat (**D**). Control cells received equal amounts of vehicle (DMSO). Cell viability assay was performed after 72 h. All data are representative of three independent experiments. Error bars indicate ± SD. Results were analyzed for statistical significance by ANOVA (Tukey's HSD drug naïve versus resistant or recovery cells comparison; NS, not significant). **E-F.** Drug naive or panobinostat and bortezomib-resistant (P + B resistant cells) or recovery cells (inhibitor removed for 30 days, P + B→ recovery) cells were seeded on 6-well plates (U87, left panel; SJG 2 middle panel; DIPG 007, right panel). The following day, cells were treated with niraparib (**E**) or selisistat (**F**) (indicated concentration) as a single agent or cotreated with FK866. Control cells received equal amounts of vehicle (DMSO). All data are representative of three independent experiments. Error bars indicate ± SD. Results were analyzed for statistical significance by ANOVA (Tukey's HSD comparison; NS, not significant).